Coupled FEM-Simulation of Magnetic Pulse Welding for Nonsymmetric Applications*

E. Uhlmann[1], A. Ziefle[1], C. König[1], L. Prasol[1]

[1] Institute for Machine Tools and Factory Management, TU Berlin, Germany

Abstract

Pulse magnetic welding can be seen as a well developed manufacturing process. However, the realization of this technology implies a high degree of knowledge concerning the intrinsic mechanisms of current transmission and force generation and accordingly a high potential of optimization can be expected. Modelling pulse magnetic forming processes requires a transient electromagnetic calculation in order to obtain the generated currents and forces. The prediction of the deforming result requires an explicit structural simulation, as the forming process is conducted in timescales of a few 100 µs. A close investigation of the relevant physical entities is carried out with ANSYS Workbench and ANSYS Emag. Furthermore, the results of the Emag calculations are used as boundary conditions for explicit structural simulations with ANSYS AUTODYN in order to predict the needed charging energy for a joining process. For validation, a comparison between simulated and measured results with respect to magnetic flux density and discharge current is shown.

Keywords

fem, pulse magnetic welding, parameter controlled bonding

---

* *This work is partly based on the results of the research project "Modellierung und Analyse des Magnetimpulsschweißens mit dem Ziel der Prozessparameteroptimierung"; the authors would like to thank the DFG for its financial support*

1 Introduction

In the last years the pulse magnetic forming process has gained an increasing attention from both manufacturing companies and research facilities [1, 2]. A considerate advance has been made in the field of simulation lately, providing a wide field of software as well the necessary hardware. Thereby the calculability of the pulse magnetic forming process has improved significantly [3]. In this paper some variants of coupled Finite Element Method (FEM) simulation approaches are presented together with necessary validation methods.

The pulsed magnetic forming process is based on the two physical effects induction and Lorentz force. The energy which is necessary for the forming process is stored in a bank of capacitors by charging them to a high voltage. By discharging the capacitors through the tool coil, the arising large currents generate an intense magnetic field inside the tool coil. This field induces eddy currents at the surface of the work piece which are running in the opposite direction compared to the primary currents in the tool coil. Due to the current inside the work piece Lorentz forces are generated, which lead to a plastic deformation of the work piece.

For pulse magnetic welding, the velocity of the deformation is used for a collision of two workpieces with high kinetic energy. Thus, the generated high pressures at the collision point lead to a cold weld of both workpieces.

2 FEM Model

As mentioned above, very high pressures as well as high strain rates occur especially near the impact regions of the workpieces. These conditions require the application of explictit FEM-software capable of modeling impact simulations. In this paper two different tool coil/work piece combinations are shown, where the first case is a axisymmetric compression of a tube onto a conical part (green) and the second case is the nonsymmetric deformation of a sheet metal (grey) towards a second fixated sheet metal. For pulse magnetic forming of metal sheets a variety of coil designs are possible. From a viewpoint of efficiency designs with many windings or with closed eddy current path are favorable [4, 5]. Conversely the primary objective for pulse magnetic welding is a high and fast acceleration which is achieved by higher currents and frequencies compared to conventional electromagnetic pulse forming processes. Thus, the majority of flat welding coils are consisting either of only one winding or an e-formed shape [6]. For demonstrational purpose a simple one-winded u-formed coil shape was chosen.

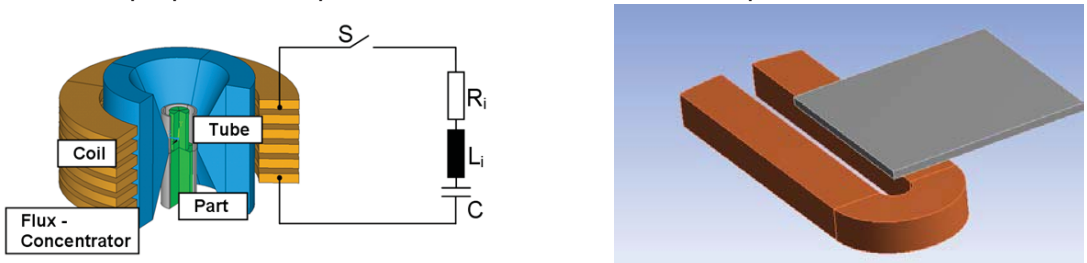

Figure 1: *left: axisymmetric case; right: nonsymmetric case*

Figure 2: *Geometries for explicit structural simulations*

2.1 Coupling Method

In order to model the pulsed magnetic forming process, there are different degrees of coupling [7]. It is possible to calculate the generated forces by an electromagnetic simulation. At loose coupled simulations the electromagnetic simulation is carried out beforehand, transferring the transient forces to the mechanical simulation afterwards [7, 8, 9, 10]. Furthermore, a sequential coupling mechanism is possible, taking into account, that the deformed work piece has an influence on the distribution of the magnetic field. Here in each time step the electromagnetic simulation and after computation of the Lorentz forces the mechanical simulation is carried out sequentially [4, 11, 12, 13, 14, 15]. Unfortunately this method is not implemented in the majority of FEM-Codes, leaving the need of a routine for interexchange of the forces calculated in the transient electromagnetic process as well as the transient deformation at each time step. For the presented simulations the loose coupling method was applied.

For a correct calculation of the forces which are generated during the process, the electromagnetic and the mechanical simulation have to be coupled as shown in figure 3.

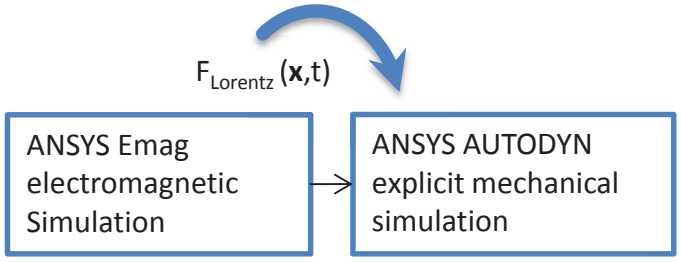

Figure 3: *Coupling method for Electromagnetic and Structural Simulation*

The transient development of the electromagnetic field and the coincidently developing Lorentz forces calculated in ANSYS Emag were used as boundary condition for an explicit structural simulation. As mentioned above, the different physical effects which have to be modelled result in different requirements for the mesh resolution. For computational efficiency the mesh of both domains are different, leading to the necessity to interpolate the data to the different mesh.

The discharging behaviour of the process needs to be analyzed during the electromagnetic simulation. Therefore an equivalent circuit of the discharging circuit is created using the assumption, that the whole discharge circuit can be modelled as a RCL – circuit consisting of one resistor, capacitor and inductor which are connected serially as depicted in figure 4. The part marked as “FEM circuit” was modelled as circuit elements, the parts marked as “FEM model”, the tool coil and the tool, were modelled as a geometrical FEM model.

2.2 Setup electromagnetic model

As only the discharging process is relevant for the forming behaviour, the charging circuit was neglected. Inner inductivity L_i and inner resistance R_i were measured at the specific pulse forming machine by carrying out short circuit tests without tool coil. For this purpose a short circuit connection was used instead of a tool coil as it is further described in [16].

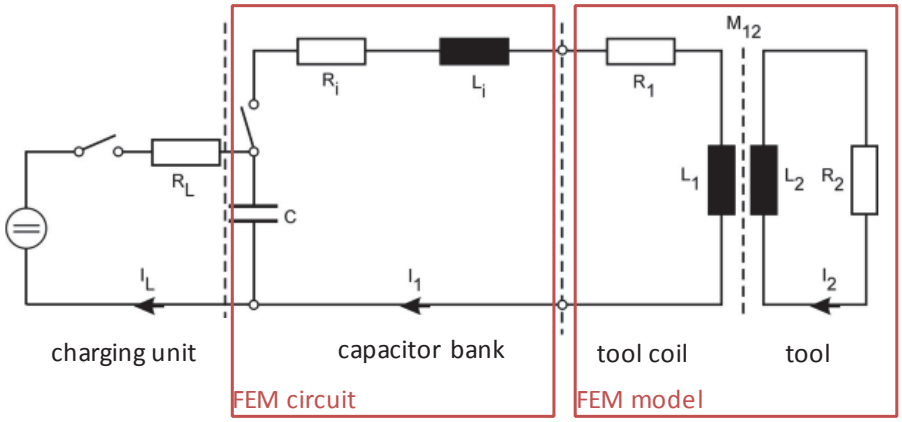

Figure 4: *Equivalent circuit diagram*

Another important aspect which needs to be considered already at the meshing stage is the skin effect δ defined by:

$$\delta = \frac{1}{\sqrt{2\pi f \mu \kappa}} \tag{6}$$

In order to accurately model the eddy currents on the surface of solid conductors it is necessary to at least resolve the skin depth with two element layers.

2.3 Setup explicit structural model

For explicit structural simulations one of the most important aspects is the relation between smallest element size and biggest possible time step through the courant condition:

$$\Delta t_{max} \leq \frac{\Delta x_{min}}{c} \tag{6}$$

Here Δt_{max} is the biggest possible time step permitting to model events approaching with longitudinal sound speed c through a mesh with the minimum element size of Δx_{min}.

Choosing a larger time step or a finer grid violating equation 6 will result in poor simulation results. Good care is also needed for a perceptive net design. Because very high deformations will occur during the collision process between both workpieces, the net needs to be prepared by initially meshing the layers in the surface of the collision side “deformed” to the contrarious direction.

3 Simulation

3.1 Axisymmetric Case

Most compression coils can be described with axisymmetric conditions. This way a considerable reduction of computation time can be achieved. Details for used materials and applied boundary conditions are referred to in table 1.

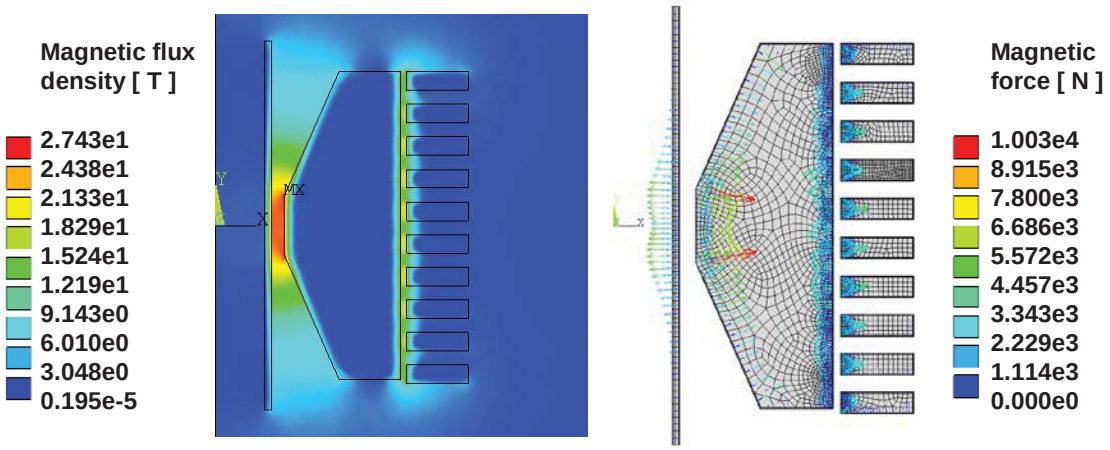

Figure 5: *Results of electromagnetic simulation; left: magnetic flux density B; right: magnetic force* F_{mag}

In figure 5 the total magnetic flux density is plotted on the left hand side. By application of the fieldformer the magnetic field between fieldformer and work piece is significantly higher than between fieldformer and tool coil. Accordingly the magnetic field inside the workpiece is almost completely vanished. On the right hand side of figure 5 the force exposure of tool coil, fieldformer and workpiece is shown. As the current density j is high in regions very close to the surfaces due to the above mentioned skin effect, also the Lorentz force F_{mag} mainly takes effect there according to the definition

$$\vec{F}_{mag} = \vec{j} \times \vec{B}. \tag{7}$$

Figure 6: *Pressure at axisymmetric case*

In figure 6 the pressure distribution after the impact of the workpiece on the conus is shown. In the contour plot on the right hand side the steep pressure maximum at the collision point is clearly visible. At this state the latent kinetic energy in the accelerated workpiece is not totally dissipated yet, the deformation process will go on and the collision point will move to the left hand side along the material surfaces.

3.2 Non symmetric three dimensional geometry

As nonsymmetric case the deformation of a metal sheet plate by use of a u-shaped flat coil was chosen. For the following graphs a cross section of the geometry is shown in order to simplify the depiction of the results.

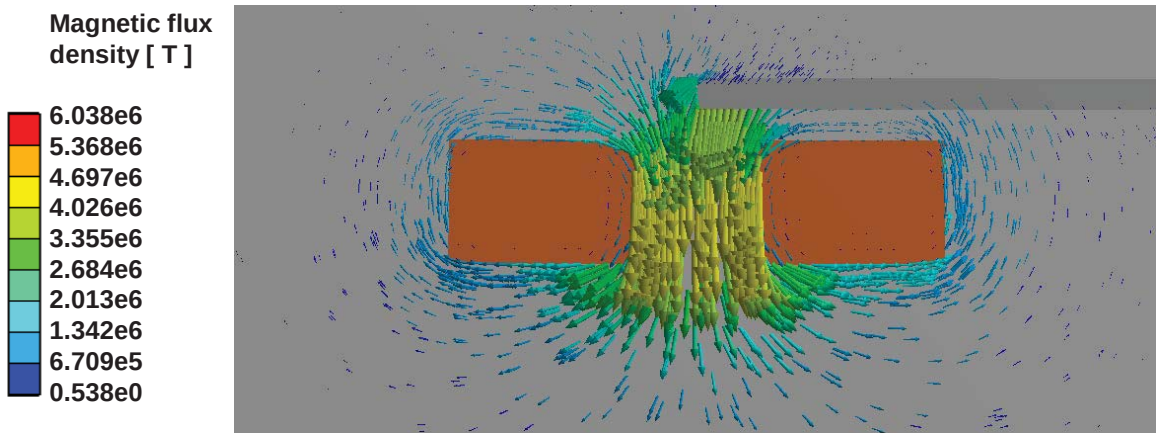

Figure 7: *Cross section of magnetic flux density B*

In figure 7 the cross section of the magnetic flux density is plotted. The magnetic field is very high between the two coil conductors, whereas the field is significantly lower in between the tool coil (orange coloured) and the metal sheet (dark grey coloured).

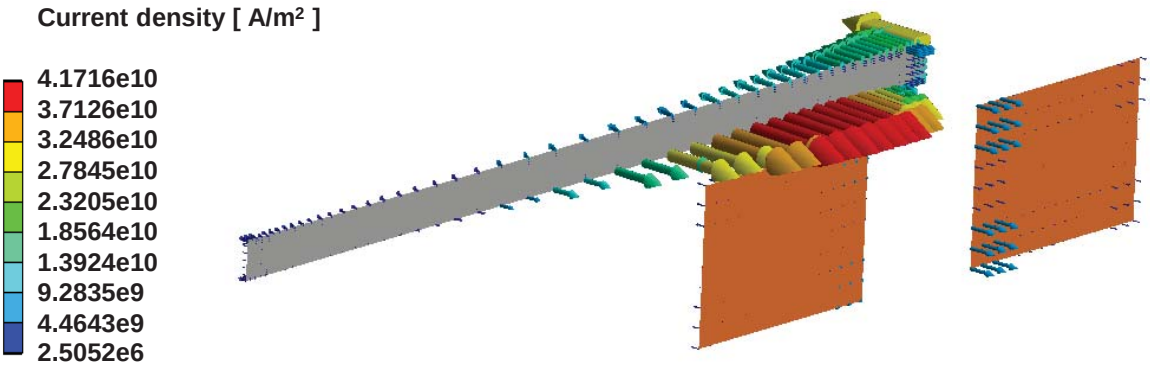

Figure 8: *Cross section of current density j*

In figure 8 the current density inside the workpiece and the tool coil is shown. Though the magnetic flux density stays low very high current densities occur inside the sheet metal.

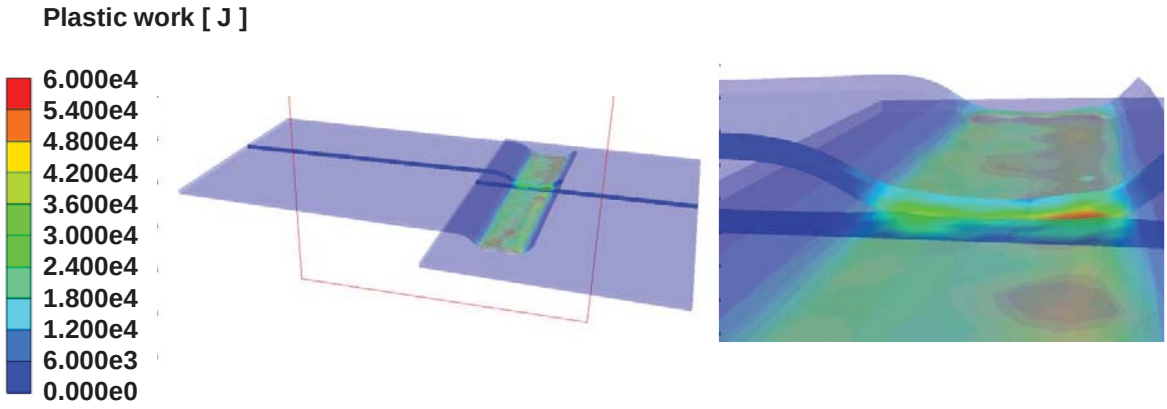

Figure 9: *Plastic work after collision*

Based on the Lorentz forces F_{mag} calculated in the electromagnetic simulation the deformation process was modelled with the explicit FEM-Software AUTODYN. In figure 9 the plastic work after the collision of the pulse magnetic deformed sheet metal plate (top) with the fixated sheet metal plate (bottom) is plotted. Especially at regions close to the collision zone very high plastic works are found.

4 Experimental Validation

4.1 Magnetic Flux Density

The magnetic flux density B was measured with a small wire coil as shown in figure 10.

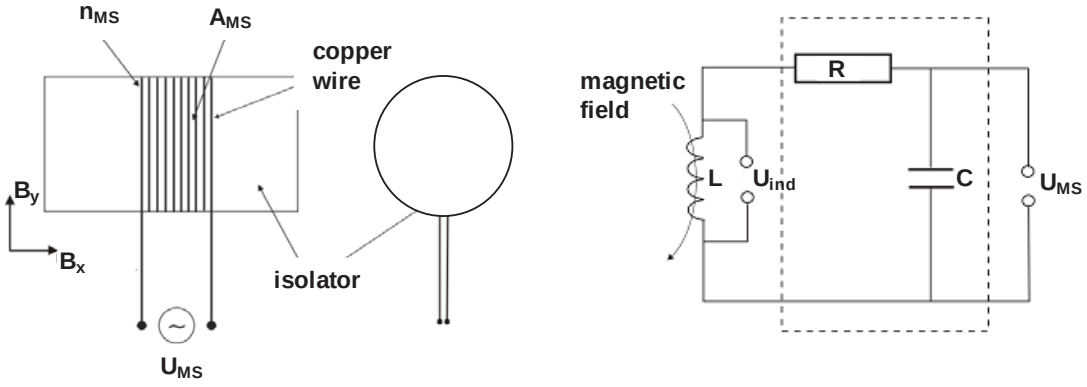

Figure 10: *Experimental setup for flux density measurements with a wire coil*

Inside of a transient magnetic field a voltage $U_{ind}(t)$ is induced which is proportional to the magnetic flux density B(t) as shown in equation 8

$$B_y(t) = \frac{RC}{n_{MS} A_{MS}} U_{MS}(t) \tag{8}$$

with resistor R and capacitor C of the measurement circuit as shown in figure 10. Furthermore A_{MS} demarks the cross section of the used wire coil whereas n_{MS} represents

the number of windings. The coil was calibrated by use of a hall sensor at magnetic flux densities of B = 1 T. The advantages of the wire coil are the usability at high frequencies f and high magnetic flux densities B. As disadvantage only the component of the magnetic flux density parallel to the wire coil axis can be measured. As the orientation of the flux density vector is approximately parallel to the tool coil axis it can be assumed that

$$\left|B_y\right|(t) \approx \left|\vec{B}\right|(t) \tag{9}$$

The validation was carried out using the same tool coil without workpiece and without fieldformer using the charging energy W_E = 1 kJ and the capacity C = 240 µF.

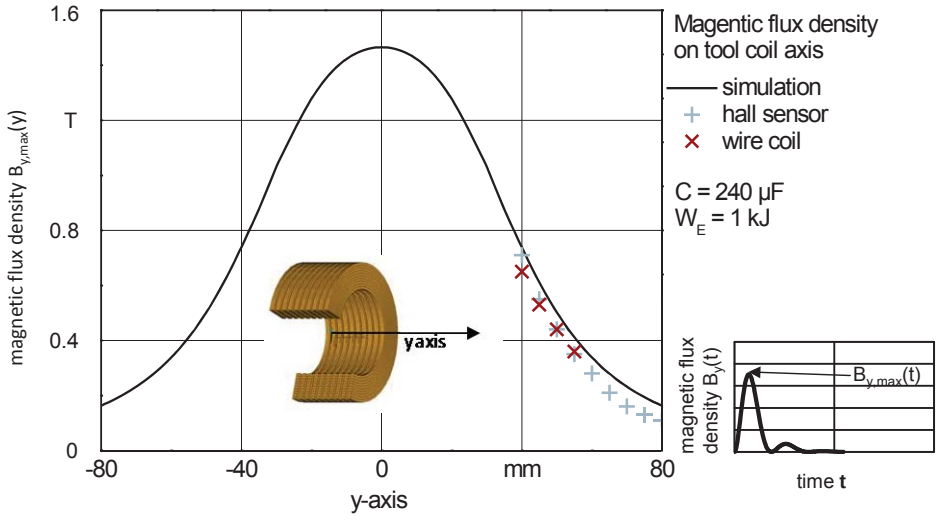

Figure 11: *Measured and simulated magnetic flux density on the rotational axis of the tool coil*

On the lower right hand side of figure 11 the local variation in time of the magnitude of the magnetic flux density B is shown. On the left hand side the development of $B_{y,max}(y)$, representing the maximum value of B_y at the location y over the tool coil axis is compared for both simulated and measured data. The hall sensor was also used for reference measurements. The results show excellent agreement to the simulated values regarding the amplitude as well as the position.

4.2 Discharge Current

The discharge current I was measured by use of a rogowski coil. By measuring the generated voltage after a passive integrator circuit, a voltage $U_{rog}(t)$ proportional to the current I(t) is measured with the following correlation

$$I(t) = m\, U_{rog}(t) \tag{9}$$

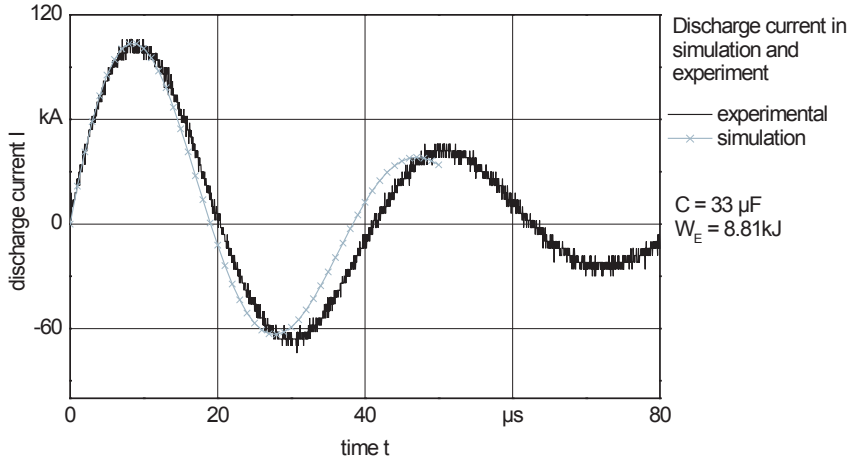

Figure 12: *Discharge Current for axisymmetric case*

In figure 12 simulated and measured discharge current are compared for the axisymmetric case. Whereas the current amplitude shows a very good accordance, the frequency of the simulated current is slightly higher than the experiment. This is due to the changing inductivity of the real system. The distance between workpiece and field former is increasing during the deformation process resulting in a change of the mutual inductance.

5 Conclusions

In this paper a short explanation of the pulse magnetic forming process was given. Furthermore the pulse magnetic forming machine was modelled with an equivalent discharge circuit, permitting to accurately simulate the discharging process depending on the capacity and charge voltage of the capacitor bank as well as on the inner resistance and inductivity of the pulse magnetic forming machine. The mentioned parts were modelled as FEM circuit, whereas the tool coil and the work piece are modelled as FEM model. Two geometries were presented including an axisymmetric compression case as well as a nonsymmetric metal sheet deformation process. The results enable a good qualitative and quantitative assessment of the inherent physical processes and enable to conduct an optimisation of geometry in order to maximize the effectiveness of the process. Location and quantity of acting forces as well as the development of current density and magnetic flux density can be analyzed. The pressure as well as the calculated plastic work are important process indicators and can eventually be used as welding criterion. The simulations were validated with magnetic flux density measurements as well as current measurements. The magnetic flux density measurements were conducted with a wire coil sensor and a hall sensor, the current measurements with a rogowski coil. Altogether a variety of approaches for simulation of pulsed magnetic forming processes were presented together with necessary validation methods.

References

[1] *Zittel, R.:* „A Historical Review of High Speed Metal Forming“. Proceedings of 4th international conference on high speed forming, 2010, Columbus, pp 2-15.

[2] *Shribman, V.:* “Magnetic Pulse Welding for Dissimilar and Similar Materials“. Proceedings of 3rd international conference on high speed forming, 2008, Dortmund, pp 13-22.

[3] *Stiemer, M.; Unger, J.; Blum, H.; Svendsen, B.:* „Fast Algorithms for the Simulation of Electromagnetic Metal Forming“. Proceedings of 3rd international conference on high speed forming, 2008, Dortmund, pp 129-140.

[4] *Uhlmann, E.; Ziefle, A.:* „Modeling Pulse Magnetic Welding Processes – An Empirical Approach“. Proceedings of 4th international conference on high speed forming, 2010, Columbus, pp 108-116.

[5] *Srinivasan, S.; Wang, H.; Taber, G.A.; Daehn, G.S.:* „Dimensional control and formability in impact forming“. Proceedings of 4th international conference on high speed forming, 2010, Columbus, pp 239-249.

[6] *Aizawa, T.*; Kashani, M.; Okagawa, K.: “Application of magnetic pulse welding for aluminum alloys and SPCC steel sheet joints”. Welding Journal Vol. 86, 2007, pp 119-124.

[7] *Bartels, G.;Schätzing, W.;Scheibe, H.-P.;Leone, M.:* “Simulation Models of the Electromagnetic Forming Process”. 2nd Euro-Asian Pulsed Power Conference, 2008, Vilnius, pp 1128-1129.

[8] *Schätzing, W.; Scheibe, H.-P.; Wollenberg, G.:* „Berechnung des magnetischen Druckes bei der Magnetumformung“. Tagungsband zum Kolloquium "Elektromagnetische Umformung", 2001, pp 33-38.

[9] *Uhlmann, E.; Ziefle, A.:* „Lösungsansätze zur Darstellung des impulsmagnetischen Schweißprozesses mittels gekoppelter FEM-Simulation“. Proceedings of Berliner Runde, 2009, pp 13-22.

[10] *Schätzing, W.; Scheibe, H.-P.; Wollenberg, G.:* „Untersuchungen zur Magnetumformung mit ANSYS“. Tagungsband zum 17. CAD-FEM Users' Meeting III, 1999, Sonthofen, pp 33-40.

[11] *Haiping, Y.U.;Chufeng, L.I.; Jianghua, D.E.N.G.:* “Sequential coupling simulation for electromagnetic-mechanical tube compression by finite element analyse”. Journal of Material Processing Technology, 2008, Vol. 209, pp 707-713.

[12] *Haiping, Y.U.; Chufeng, L.I.:* “Effects of current frequency on electromagnetic tube compression”. Journal of Material Processing Technology, 2009, Vol. 209, pp 1053-1059

[13] *Bartels, G.; Schätzing, W.; Scheibe, H.-P.; Leone, M.:* „Models for Electromagnetic Metal Forming”. Proceedings of the 3rd International Conference on High Speed Forming, Dortmund, 2008, pp 121-128.

[14] *Demir, O.K.; Psyk, V.; Tekkaya, A.E.:* “Simulation of tube wrinkling in electromagnetic compression”. Prod. Eng. Res. Devel., 2010, Vol. 4, pp 421-426.

[15] Brosius, A.: “Verfahren zur Ermittlung dehnratenabhängiger Fließkurven mittels elektromagnetischer Rohrumformung und iterative Finite-Elemente-Analysen”. Dissertation, 2005, Technische Universität Dortmund.

[16] *Uhlmann, E.; Ziefle, A.:* „Simulation approaches for pulse magnetic forming“. Prod. Eng. Vol. 5. Issue 6, pp 659-665.

Appendix A Additional Information

A.1 Boundary Conditions and Material Data

In table 1 the relevant boundary conditions as well as the used material properties are enlisted.

Property	2D case	3D case
Material data		
coil	copper	copper
electrical conductivity	56 MSm^{-1}	56 MSm^{-1}
relative permeability	1	1
field former	EN AW 6060	-
electrical conductivity	66 MSm^{-1}	-
relative permeability	1	-
workpiece	AL 1100-O	
electrical conductivity	36 MSm^{-1}	36 MSm^{-1}
relative permeability	1	1
material model	Steinberg Guinan	Steinberg Guinan
Boundary Conditions		
capacity	240 µF	240 µF
resistance	13,8 mΩ	25 mΩ
charging energy	9 kJ	4,8 kJ
symmetry	2D axial	-
surrounding temperature	25°C	25°C
Process parameters		
discharge frequency	7,4 kHz	29,7 kHz
skin depth (work piece)	0,956 mm	0,482 mm

Table 1: *Boundary conditions and material data used for carried out simulations*